Available online at www.sciencedirect.com
SCIENCE DIRECT®
Journal of Magnetic Resonance 178 (2006) 42–55
JMR Journal of Magnetic Resonance
www.elsevier.com/locate/jmr

EasySpin, a comprehensive software package for spectral simulation and analysis in EPR

Stefan Stoll *, Arthur Schweiger

Physical Chemistry Laboratory, ETH Hönggerberg, CH-8093 Zürich, Switzerland

Received 24 June 2005; revised 29 August 2005
Available online 26 September 2005

Abstract

EasySpin, a computational package for spectral simulation and analysis in EPR, is described. It is based on Matlab, a commercial technical computation software. EasySpin provides extensive EPR-related functionality, ranging from elementary spin physics to data analysis. In addition, it provides routines for the simulation of liquid- and solid-state EPR and ENDOR spectra. These simulation functions are built on a series of novel algorithms that enhance scope, speed and accuracy of spectral simulations. Spin systems with an arbitrary number of electron and nuclear spins are supported. The structure of the toolbox as well as the theoretical background underlying its simulation functionality are presented, and some illustrative examples are given.

Keywords: EPR; ENDOR; Breit–Rabi

1. Introduction

In EPR spectroscopy (including ENDOR and pulse EPR), the extraction of information on structure and dynamics from experimental data heavily relies on computerized data processing, numerical spectral simulations and iterative parameter fittings. While data processing software is widely available and fitting algorithms are well established, a general and flexible simulation environment for EPR spectroscopy is still lacking.

Numerical simulations of EPR spectra are usually performed with three intentions: (1) systematic study of the dependencies of spectral features on the magnetic parameters, (2) predictions whether a new experiment will give new information, and (3) accurate parameter extraction from experimental spectra.

Most currently available EPR simulation programs have substantial limitations. Many programs are tailored to special experiments or/and spin systems. They cannot be extended or modified easily. Visualization capabilities are rarely included, and if available, they are again restricted to special types of display. Programs with graphical interfaces, though excellent [1], have the disadvantage that their interface is too inflexible to permit application to new or unusual simulation problems. Most programs (such as [2,3]) use approximations in their simulation algorithms and do not usually check the validity of the approximations for the spin systems at hand, so that incorrect spectra can be obtained. For a range of systems and experiments (many-electron spin systems, ENDOR of high-spin systems, ESEEM), no general simulation programs are available.

We have taken a general approach to the problem and have written EasySpin, a computational EPR package that eliminates most of the disadvantages mentioned above. It provides all necessary tools from basic data processing and visualization functionality to spectral simulation. It is based on Matlab (The Mathworks, Natick, MA, USA), a commercial programmable numerical and visualization software environment, for the following reasons: The programming language of Matlab is based on matrices and very efficient matrix algorithms, thus relieving the spectroscopist of the implementation of these basic numerical types

* Corresponding author. Fax: +41 44 632 1021.
E-mail address: stoll@phys.chem.ethz.ch (S. Stoll).

1090-7807/$ - see front matter © 2005 Elsevier Inc. All rights reserved.
doi:10.1016/j.jmr.2005.08.013

Table 1
Selected EasySpin functions

Function	Description
`sop`	Spin matrices
`stev`	Extended Stevens operator matrices
`levels`	Energy levels
`resfields`	Resonance fields
`pseumod`	Pseudo-modulation
`ctafft`	Cross-term averaged FFT
`apowin`	Various apodization windows
`eprload`	Import of experimental data
`eulang`	Conversion from rotation matrices to Euler angles
`pepper`	Solid-state cw EPR spectra simulation
`garlic`	Isotropic cw EPR spectra simulation
`salt`	ENDOR spectra simulation

and procedures. Matlab has a simple syntax, and any new experimental idea can be coded and evaluated very quickly with a few additional EPR-specific functions. Visualization capabilities are extensive and very flexible. Matlab is available for many different platforms, so that portability is guaranteed within multiple-platform networks as employed in our laboratory.

EasySpin consists of over 80 Matlab functions performing a variety of EPR-related tasks. The functions are divided into two categories (see Table 1). Functions from the larger and more basic category provide the core functionality necessary for computational EPR. These functions can be freely combined to write programs tailored to special experiments and problems. Built on this foundation, a small number of general and robust high-level functions for spectral simulation are provided, which implement a series of substantial algorithmic improvements. In all, EasySpin represents a powerful, highly flexible and integrated analysis and simulation environment for EPR spectroscopists.

In the following we describe the working of the major features of the EasySpin toolbox in terms of the EPR theory involved. Section 2 reviews the algorithms underlying the implementation of the EPR and ENDOR simulation functionalities. Section 3 provides details about other functions, and in Section 4, a few representative examples illustrate some of the features of the toolbox.

2. Spectrum simulations

EasySpin includes several high-level functions performing common simulation tasks: `pepper` for solid-state EPR spectra of both single crystals and disordered systems, `garlic` for solution and rapid-motion EPR spectra, and `salt` for solid-state ENDOR spectra. In the following we outline the inner working of these simulation functions and present a number of algorithmic improvements [4,5].

2.1. Solid-state EPR

The simulation of field-swept cw EPR spectra of single crystals and disordered systems (powders, frozen solutions, and glasses) can be achieved by using the function `pepper`.

2.1.1. Spin Hamiltonian

The cw EPR simulation function `pepper`, and EasySpin in general, supports spin systems with $N_e \geqslant 1$ electron spins and $N_n \geqslant 0$ nuclear spins governed by the spin Hamiltonian

$$\begin{aligned}\mathscr{H} = {} & \frac{\beta_e}{h}\boldsymbol{B}^T\sum_{k=1}^{N_e} g_k\boldsymbol{S}_k - \frac{\beta_n}{h}\boldsymbol{B}^T\sum_{k=1}^{N_n} g_{nk}\boldsymbol{I}_k \\ & + \sum_{k=1}^{N_e}\sum_{q=1}^{N_n}\boldsymbol{S}_k^T A_{kq}\boldsymbol{I}_q + \sum_{q=1}^{N_n}\boldsymbol{I}_q^T Q_q\boldsymbol{I}_q \\ & + \sum_{k=2,4,6}\sum_{q=-k}^{k} B_{kq}O_{kq} + \sum_{k=1}^{N_e}\sum_{q=1}^{N_e}\boldsymbol{S}_k^T X_{kq}\boldsymbol{S}_q. \end{aligned} \tag{1}$$

The spin Hamiltonian $\mathscr{H}$ as well as all the state energies and interaction parameters except g and g_n are in frequency units (MHz). The symbols have their usual meaning (see e.g. [6]). The first two terms describe the Zeeman interactions of the electron and nuclear spins with the external magnetic field $\boldsymbol{B}$. The g_n values are assumed to be isotropic. The third and fourth term represent the hyperfine and the nuclear quadrupole interaction. The fifth term, which describes higher-order zero-field interactions of one electron spin, is a linear combination of Stevens operators O_k^q [7]. This term also contains the standard zero-field splitting more commonly written as

$$\boldsymbol{S}^T D\boldsymbol{S} = D\left[S_z^2 - S(S+1)/3\right] + E(S_x^2 - S_y^2) \tag{2}$$

with $D = 3B_{20}$ and $E = B_{22}$. The last term in Eq. (1) describes a general interaction between two electron spins. The interaction matrix X is the sum of an isotropic exchange and a traceless symmetric dipolar interaction term.

All interaction tensors may have arbitrary orientations with respect to a molecule-fixed frame M, which is used as the frame of reference by all EasySpin simulation functions. The tensors are specified via their principal values and the Euler angles [8] defining the orientation of the principal frames in the molecule-fixed frame M. g, A, and X may be asymmetric, in which case all nine elements of the matrices have to be specified. The orientation of the paramagnetic centre with respect to the laboratory frame L is defined by the three Euler angles ϕ, θ, and χ. The static magnetic field $\boldsymbol{B}$ is oriented along the laboratory z axis (zL). The unit vector along this orientation in the molecular-frame representation is $\boldsymbol{z}_L^T = (\cos\phi\sin\theta, \sin\phi\sin\theta, \cos\theta)$.

The spin Hamiltonian is a linear function of the magnetic field

$$\mathscr{H}(B) = F + \boldsymbol{B}^T\boldsymbol{G} = F + B\boldsymbol{z}_L^T\boldsymbol{G} = F + BG_{zL}, \tag{3}$$

where F collects all field-independent terms and $\boldsymbol{G}^T = (G_{xM}, G_{yM}, G_{zM})$ is the vector operator of spin magnetic moments

$$\frac{\beta_e}{h}\sum_{k=1}^{N_e} g_k \boldsymbol{S}_k - \frac{\beta_n}{h}\sum_{k=1}^{N_n} g_{nk}\boldsymbol{I}_k. \quad (4)$$

In a matrix representation, F and the three elements of $\boldsymbol{G}$ are matrices. Since they are independent of $\boldsymbol{B}$, they need to be computed only once for a powder simulation.

The field-dependent energies of the spin states are given by the eigenvalues of the Hamiltonian $\mathscr{H}(\boldsymbol{B})$. It is known [9] that the energies $E_u(\boldsymbol{B})$ of different states are different for all fields $\boldsymbol{B}$ except at isolated points, where two or more state energies are degenerate. These points are so-called crossing points and lie along symmetry axes of the point group of the spin Hamiltonian [10]. In the vicinity of crossing points, the state energies come very close, and the eigenstates change rapidly. Such anticrossing regions can occur even without a crossing point. The energies $E_u(\boldsymbol{B})$ are differentiable functions of $\boldsymbol{B}$ everywhere except at crossing points. As a consequence, the sorting of the energies and states in ascending order $E_1 \leqslant E_2 \leqslant \cdots \leqslant E_N$ is unique, in contrast to assumptions made by some authors [2,11,12].

2.1.2. Resonance fields

During a field-swept EPR experiment, the magnitude B of the magnetic field and consequently the spin Hamiltonian $\mathscr{H}(B)$ changes continuously. This is not the case in experiments where the frequency ν_{mw} is swept. Whereas resonance *frequencies* are easily obtained as differences of eigenvalues of the Hamiltonian, resonance *fields* are given only implicitly by the coupled equations

$$\mathscr{H}(B)|u\rangle = E_u|u\rangle \quad \mathscr{H}(B)|v\rangle = E_v|v\rangle \quad \Delta_{uv} = E_v - E_u = \nu_{mw} \quad (5)$$

with $E_v > E_u$. This implies qualitative differences between the two types of spectra. In contrast to the frequency-swept spectrum where there is exactly one resonance frequency per state pair (transition), the field-swept spectrum can also have zero (if $\Delta_{uv}(B) > \nu_{mw}$ for all B), one or more than one resonance field (if $\Delta_{uv}(0) > \nu_{mw}$ and $\Delta_{uv}(B) < \nu_{mw}$ for some B) per state pair. The latter are called looping transitions [13].

Eq. (5) cannot be solved directly in state space, neither analytically nor numerically. However, they can be cast into a generalized eigenvalue problem in Liouville space, yielding the resonance fields as eigenvalues [14]. Though being most general and involving highly sparse matrices, this approach is computationally too costly, since the matrix dimensions, as well as the complexity order of the diagonalization algorithm, are squared compared to the state space problem.

In state space, the general numerical solution of Eq. (5) requires iterative methods. Many different schemes have been proposed. Extrapolative methods use either frequency-shift [1] or classical perturbation theory [2]. Homotopy methods make use of a least-squares method [15] or Newton–Raphson steps combined with Rayleigh quotient iteration [16]. Many approaches apply standard root finding algorithms [10,11].

For a given pair of states u and v, all these methods produce at most one resonance field. To find multiple resonance fields for a state pair, the only method described in the literature is to use a set of usually equally spaced starting fields for the iteration method of choice. A group of methods extends this multiple-field approach and constructs a cubic spline [13,17] or a Chebyshev polynomial [18] model of the energy level diagram to obtain the resonance fields. The number and positions of the starting fields are set manually. If looping resonances crowd in a small field range, the accuracy of the resonance fields depends critically on the placement of the starting fields.

The EasySpin functions `resfields` and `pepper` implement a new energy level modeling procedure based on iterative adaptive bisections, as described in detail elsewhere [5]. This procedure, which finds all resonance fields within a given field range $B_{min} \leqslant B \leqslant B_{max}$, works as follows.

The method starts with the interval $[B_{min}, B_{max}]$. First, state energies E_u and their derivatives $\partial E_u/\partial B$ at the interval borders are computed by diagonalizing the associated Hamiltonians. The derivatives are obtained using Feynman's theorem

$$\frac{\partial E_u}{\partial B} = \left\langle u\left|\frac{\partial H}{\partial B}\right|u\right\rangle = \langle u|G_{zL}|u\rangle. \quad (6)$$

The results are used to compute a Hermite spline representation of the energy level diagram across the field range. Next, the Hamiltonian is diagonalized at the centre of the interval $B_{cen} = (B_{min} + B_{max})/2$, and the resulting energies are compared to the ones obtained by spline interpolation from the two boundary field values. If the error is below a certain threshold or resonances can be excluded, the modelling is stopped. If not, the two sub-intervals $[B_{min}, B_{cen}]$ and $[B_{cen}, B_{max}]$ are refined by diagonalizing the Hamiltonians at their centre fields and checking against the interpolated approximations. This subdivision is repeated until all interval centre errors are below the threshold.

The result of this procedure is a faithful cubic spline representation of the energy level diagram over the field range of interest, as illustrated in Fig. 1. In regions of anticrossings, the interval density is higher than in regions with linear energy level dependencies. For high-field situations, three diagonalizations are sufficient. Only in cases with very complicated $E_u(B)$ dependencies, such as the one shown in Fig. 1, the number of intervals exceeds 10.

From this spline representation, resonance fields are obtained by analytically solving the cubic equations $\Delta_{uv}(B) = \nu_{mw}$ for all intervals with potential resonances. Multiple resonance fields for a state pair are thus easily and automatically detected. Eigenvectors are obtained by linear interpolation using the computed eigenvectors at the interval boundaries [5].

For large spin systems, the spin Hamiltonian matrices are very large. For example, the spin system of Cu(II)phthalocyanine consisting of one electron spin $S = 1/2$, a copper nucleus with spin $I = 3/2$ and four ^{14}N

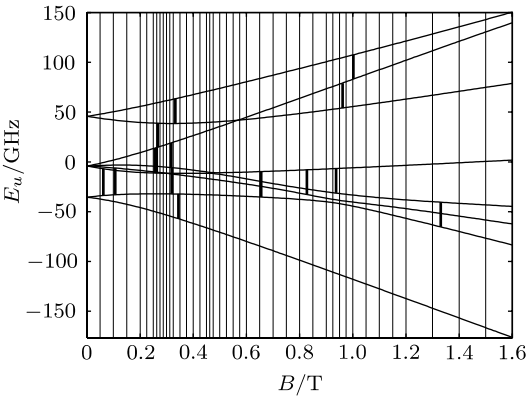

Fig. 1. Segmentation and resonance fields for Tb^{4+} in a ThO_2 single crystal [19] obtained by adaptive iterative bisection. The 43 segments contain 15 resonance fields with a maximum resonance field error of 4.5 μT.

nuclei with $I = 1$ has 648 states, and a full simulation requires diagonalizations of large 648×648 matrices. To reduce the computational effort, nuclei weakly coupled to the electron spin can be treated using first-order perturbation theory, provided that their hyperfine interaction is much smaller than the microwave frequency and larger than the nuclear Zeeman and the nuclear quadrupole interactions. In this case, the resonance fields are computed for the core system $S = 1/2$, $I = 3/2$ (matrix size 8×8), and resonance field shifts are added for the four nitrogen nuclei. An important aspect of the implementation of the first-order treatment is that the EasySpin function automatically determines whether the approximation is applicable or not.

2.1.3. Intensities

After having obtained the resonance field and the eigenvectors of a transition, the associated line intensity is computed. In the commonly used first-order perturbation limit, the intensity is given by

$$A_{uv}^{(\mathrm{EPR})} = M_{uv}(\boldsymbol{B}_1)\beta_{uv}\gamma_{uv} \tag{7}$$

with the transition rate M_{uv}, the polarization factor β_{uv} and the frequency-field conversion factor γ_{uv}.

The transition rate M_{uv} depends on the strength and orientation of the microwave field $\boldsymbol{B}_1$. In standard cw EPR experiments, $\boldsymbol{B}_1$ is perpendicular to the static field $\boldsymbol{B}$, that is, parallel to the x axis of the laboratory frame (xL). The transition rate is then given by

$$M_{uv}^{(\perp)} = \left|\langle v|\boldsymbol{B}_1^{\mathrm{T}}\boldsymbol{G}|u\rangle\right|^2 = B_1^2|\langle v|G_{x\mathrm{L}}|u\rangle|^2. \tag{8}$$

$\boldsymbol{B}_1$ and hence $G_{x\mathrm{L}}$ depend on all three Euler angles ϕ, θ, and χ. For a powder spectrum, the contribution to the signal intensity from all systems with a single orientation of $\boldsymbol{B}$ can be obtained by integrating $M_{uv}^{(\perp)}$ analytically [20] over χ yielding

$$\int_0^{2\pi} M_{uv}^{(\perp)}\mathrm{d}\chi = \pi B_1^2\left[|\langle v|G_{x\mathrm{L}}|u\rangle|^2 + \left|\langle v|G_{y\mathrm{L}}|u\rangle\right|^2\right]. \tag{9}$$

Note that, due to this integration, the resulting spectrum is neither a single-crystal spectrum nor a 'single-orientation' spectrum.

In parallel-mode cw EPR, $\boldsymbol{B}_1$ is parallel to $\boldsymbol{B}$, along the laboratory z axis. In this case the transition rate is independent of χ

$$M_{uv}^{(\parallel)} = B_1^2|\langle v|G_{z\mathrm{L}}|u\rangle|^2 \tag{10}$$

with an additional pre-factor of 2π for the integral over χ in the case of a powder.

The second factor determining the EPR line intensity is the polarization factor β_{uv}, which is proportional to the population difference between the states u and v. At thermal equilibrium, it is determined by the temperature-dependent Boltzmann distribution

$$\beta_{uv}(T) = \frac{\exp(-E_u/\alpha) - \exp(-E_v/\alpha)}{\sum_q \exp(-E_q/\alpha)}, \quad \alpha = k_{\mathrm{B}}T/h. \tag{11}$$

If the high-temperature criterion $k_{\mathrm{B}}T \gg h|E_q|$ is met, $\exp(-E_q/\alpha) \approx 1 - E_q/\alpha$, and β_{uv} is proportional to the energy difference Δ_{uv}. Since $\Delta_{uv} = \nu_{\mathrm{mw}}$, β_{uv} is identical for all transitions and can thus be dropped in this case. The high-temperature approximation holds in all experimental situations except at low temperatures (<10 K) and high spectrometer frequencies (≥95 GHz). EasySpin uses Eq. (11) without any approximation in all cases.

In some experimental situations, e.g., excited triplet states, the populations are not in thermal equilibrium. In such a case, `pepper` and `resfields` compute the level populations for the polarization factor β_{uv} as linear combinations of the user-supplied populations of the zero-field states [21].

The third factor in Eq. (9), the frequency-field conversion factor γ_{uv}, is discussed in Section 2.1.6.

2.1.4. Transition selection

For most systems, only a small fraction of all possible transitions are observable in an EPR spectrum, since the great majority of transitions are forbidden (e.g., $\Delta m_{\mathrm{I}} \neq 0$ or $\Delta m_{\mathrm{S}} \neq 1$ in the high-field limit). It is therefore a waste of time to compute all possible resonances within a specified field range [17]. Only line positions and intensities of transitions which significantly contribute to the final spectrum should be computed. This is not necessary for single-crystal spectra, but becomes essential for powder spectra, where spectra for a large number of differently oriented paramagnetic centres are computed.

The obvious way of selecting transitions based on the EPR selection rules and their nominal Δm_{S} and Δm_{I} values can only be applied in the high-field limit where all the eigenstates are almost pure (electronic and nuclear) Zeeman states. A more viable approach [22] is to estimate average transition rates for a small number of orientations $\boldsymbol{z}_{\mathrm{L}}(\phi,\theta)$ for all transitions at B_{cen}. Only state pairs with an average transition rate above a given threshold are then used in the simulation itself. This pre-selection runs into

problems in the presence of sharp level anticrossings along θ or ϕ, which occur in systems with coupled electron spins or, more commonly, in systems with several nuclei with comparable hyperfine couplings. In such cases, some transitions are allowed only for a very small orientational range, and forbidden outside. Such transitions will then be erroneously excluded.

EasySpin takes a more failsafe approach, if sharp anticrossings are encountered. As in the general case, transitions are selected based on their transition rates at B_{cen}, but for every orientation separately, i.e., for every orientation anew in a powder simulation. The eigenvectors at B_{cen} necessary to compute the transition matrix elements are already available from the adaptive modelling procedure described in the previous section. Again, only transitions with relative amplitudes above a given threshold of $\approx 10^{-4}$ are selected.

The problem of anticrossings in systems with several nuclei can be circumvented by treating them perturbationally, as discussed previously. However, the couplings have to be small enough in order not to compromise the accuracy of line positions and intensities.

2.1.5. Line broadening

In the solid state, spin systems cannot usually be described by a single set of spin Hamiltonian parameters. First, the paramagnetic centres interact through space. Since they are randomly oriented and distributed and the couplings are small for magnetically diluted samples, the resulting splittings are not observable and contribute to the linewidths. Second, many hyperfine couplings due to nuclei in and around a single paramagnetic centre are too small and too numerous to be resolved. Again, their cumulative effect consists of an additional broadening of the spectral lines. Third, different centres experience slightly different molecular environments due to structural strains acting on the molecule from the host (glass or frozen solvent). This gives rise to anisotropic distributions in the magnetic parameters. Strain distributions are usually Gaussian and result in an additional broadening of the resonance lines.

The inhomogeneous broadenings due to unresolved splittings from nuclear and electron spins are accounted for by a residual linewidth Γ_{res}. Parameter distributions can be included in a simple way, if they are narrow. In this case, their influence on the transition frequencies Δ_{uv} can be approximately treated as a linear first-order perturbation effect. The linewidth Γ_p of a transition due to a Gaussian distribution of the magnetic parameter p is then proportional to the width σ_p of the corresponding parameter distribution

$$\Gamma_p(\Delta_{uv}) = \sigma_p \frac{\partial \Delta_{uv}}{\partial p} = \sigma_p \left[\left\langle v \left| \frac{\partial \mathscr{H}}{\partial p} \right| v \right\rangle - \left\langle u \left| \frac{\partial \mathscr{H}}{\partial p} \right| u \right\rangle \right]. \qquad (12)$$

The linewidth parameters Γ_{res} and σ_p are orientation-dependent. For a given orientation, the total Gaussian linewidth results from the convolution of the residual broadening and the various strain broadenings

$$\Gamma_{\text{tot}}^2 = \Gamma_{\text{res}}^2 + \sum_p \Gamma_p^2, \qquad (13)$$

which are assumed to be statistically independent.

The EasySpin cw EPR simulation function `pepper` supports anisotropic broadening in frequency domain to describe unresolved couplings, g/A strain [23–25], and D/E strain [26,27]. The lineshape is assumed to be Gaussian in all cases. Since, for certain applications, the detailed modelling of the linewidth is not necessary, a simple isotropic convolutional broadening in the field domain is also available.

2.1.6. Frequency-to-field conversion

The inhomogeneous linewidths discussed above are defined in the frequency domain. Thus, they describe broadenings for frequency-swept spectra, i.e., for a cross section along ν_{mw} of the two-dimensional spectral function $S(B, \nu_{\text{mw}})$. However, a field-swept spectrum corresponds to a cross section of $S(B, \nu_{\text{mw}})$ along B. Hence, the field-domain line shape is a projection of the frequency-domain line shape determined by the dependence of Δ_{uv} on B [28]. If $\Delta_{uv}(B)$ is linear across the entire frequency-domain line shape, the projection results in a simple broadening of the line governed by the generalized $1/g$ factor [29]

$$\gamma_{uv} = \left| \frac{\partial \Delta_{uv}}{\partial B} \right|^{-1} = \frac{1}{|\langle v|G_{z\text{L}}|v\rangle - \langle u|G_{z\text{L}}|u\rangle|}. \qquad (14)$$

The maxima of the frequency- and the field-domain line shapes are identical. If an area-normalized line shape function is used, the field-domain intensity has to be multiplied by γ_{uv} as well (see Eq. (7) in Section 2.1.3).

If broadenings in frequency domain are large, or if resonances are close to anticrossings, $\Delta_{uv}(B)$ is significantly curved over the region of the frequency-domain line shape. As a consequence, in such cases, line shapes symmetric in frequency domain transform to asymmetric line shapes in field domain [30]. Though line shapes of looping transitions in single-crystal spectra may be affected significantly by this non-linearity, its impact on powder spectra is usually negligible [13].

Therefore, the function `pepper` uses the linear approximation based on Eq. (14). In principle, higher derivatives such as $\partial^2 \Delta_{uv}/\partial B^2$ are available from the cubic spline model obtained in the adaptive modelling and could be used in a more general non-linear frequency-to-field conversion [13]. However, if non-linear effects are significant, an explicit averaging loop over the spin Hamiltonian parameter distribution responsible for the broadening can easily be written.

2.1.7. Powder averages

For powder spectra, the computations described in the previous sections have to be performed for a large set of different orientations $z_{\text{L}}(\phi,\theta)$ uniformly distributed over the unit sphere. Since the spectrum of any spin system is invariant under inversion of the external magnetic field, the computation can be restricted to one hemisphere

(usually $0 \leqslant \theta \leqslant \pi/2$). The spectrum may possess additional symmetry. All symmetry operations on the magnetic field vector in the molecular frame, which leave the eigenvalues of the Hamiltonian invariant constitute one of the centrosymmetric point groups $D_{\infty h}$, O_h, T_h, C_i, S_6, D_{3d}, D_{xh}, C_{xh}, with $x = 2,4,6$. In `pepper`, the point group of a given spin system is automatically determined by examining the symmetries and relative orientations of the various interaction matrices of the spin Hamiltonian.

Depending on the point group, the orientational integration can be limited to a subregion of the hemisphere. For example, a spin system with two non-collinear axial tensors has C_{2h} symmetry, and two octants are sufficient to get the full powder average. An $S = 1/2$ spin system with an orthorhombic g tensor has D_{2h} symmetry, and the integration can be limited to one octant. For an axial system, the weighted integration over a quarter of a meridian ($\phi = 0$ and $0 \leqslant \theta \leqslant \pi/2$) results in the full powder spectrum.

To integrate over the symmetry subregion, resonance data are computed for a set of orientations $\boldsymbol{z}_L(\phi,\theta)$ which homogeneously cover the region. Such sets of knots are termed spherical codes or spherical grids. For an extensive comparison of the various grids see [31,32]. The grid used in EasySpin is a simple triangular one also used in the program Sophe [1]. In the case of one octant, the angles are given by

$$\phi_{k,q} = \frac{\pi}{2}\frac{q}{k} \quad \theta_{k,q} = \frac{\pi}{2}\frac{k}{K-1} \tag{15}$$

with $k = 0,\ldots,K-1$ and $q = 0,\ldots,k$, where K specifies the number of knots along a quarter of a meridian. For one octant, the grid contains $K(K+1)/2$ knots. Advantages of the triangular grid defined in Eq. (15) are the simple construction, the possibility to easily interpolate along ϕ, and the relatively high uniformity [32].

Fig. 2 depicts a one-octant grid for $K = 12$. The immediate neighborhood of each knot, i.e., the region of all points that are closer to that knot than to any other, has the shape of a spherical polygon and is called its Voronoi cell. The areas of these Voronoi cells are the appropriate weights, which have to be used if the powder spectrum is constructed by summing over the knot spectra. Fig. 2 also shows the Delaunay triangulation of the grid resulting in a set of spherical triangles with three knots at the vertices of each triangle. These Delaunay triangles are used in the projective construction of the spectrum (see Section 2.1.8).

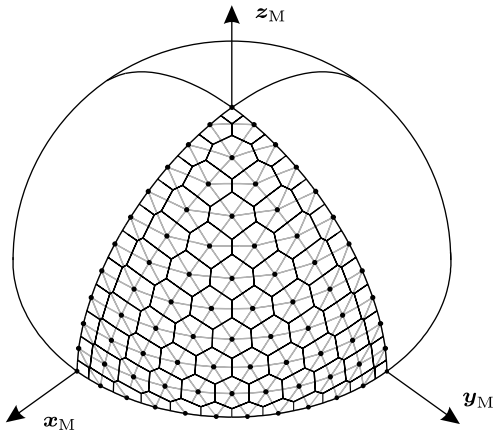

Fig. 2. Orientational grid over one octant for a spin system with D_{2h} symmetry. $K = 12$, 78 knots. Voronoi cells and Delaunay triangles are shown.

After a grid Ω_1 appropriate to the symmetry of the Hamiltonian has been set up, resonance fields, line intensities and linewidths are computed for all knots. This first step is computationally quite expensive, since for each orientation it involves several matrix diagonalizations and multiplications. To reduce the computational burden, some methods (e.g. [16]) use the fact that resonances of two close orientations do not differ substantially and take the resonance fields and eigenvectors obtained for one orientation as starting values for an iterative determination of those at nearby orientations.

In a second step, a surface representation of the resonance fields $B(\phi,\theta)$, transition rates and linewidths is constructed using bivariate tensor product cubic splines with boundary conditions depending on the symmetry.

The spline surface representations are evaluated over an orientational grid Ω_2 much finer than the original Ω_1 to obtain new values for positions, intensities and widths. This interpolation is much faster than the explicit quantum mechanical calculation. It it used to increase the number of computed knots by a factor of 10–100 in a fraction of time needed for the quantum mechanical computation. The computationally expensive orientational grid Ω_1 has thus to be only as fine as to allow the splines to closely approximate the exact surfaces. If the grid is too coarse, the final spectrum will be distorted.

The interpolation procedure is similar to the one used in the program Sophe [1], where a one-dimensional trigonal instead of a two-dimensional cubic rectangular interpolation is used. Although Sophe's interpolation is one-dimensional and hence faster for a given grid resolution, the bivariate tensor product spline approach used in EasySpin is more accurate, since correct boundary conditions along θ and ϕ can be imposed. As a consequence, Ω_1 can be coarser. In `pepper`, the resolution of the first coarse grid as well as the interpolation factor is customisable by the user. A starting grid with $K_1 \approx 20$ and a refining grid with $K_2 \approx 5K_1$ are sufficient for most spectral simulations.

In the case of looping transitions, the bivariate spline interpolation method is not applicable, since looping transitions lack resonance fields for some orientations. In this case, a higher resolution of Ω_1 has to be chosen.

Besides randomly oriented disordered systems, EasySpin also supports the simulation of paramagnetic centres partially oriented in frozen nematic liquid crystals [33]. In this case, the spherical grid and interpolation scheme is used exactly as described above, and an additional orientation-dependent factor is included in the intensity expression Eq. (7).

2.1.8. Spectrum construction

In the final stage of the spectral simulation, the absorption spectrum is constructed from the resonance data (positions, intensities, and widths). For single crystals and isotropic systems this amounts to a simple summation of Gaussian line shapes with different positions, areas and widths.

For an anisotropic powder spectrum, two different methods can be employed. The first one, used by almost all EPR simulation programs, comprises the summation of the single-crystal spectra from all the computed orientations, weighted by the Voronoi cell areas (see Fig. 2 and [4]) of the knots or their estimates [1]. This can lead to ripples in the spectrum ("simulation noise") if the number of knots is not sufficiently large, since contributions from the orientational regions between the knots are missing in the spectrum. The method can be improved by convoluting the linewidth with an additional broadening, which accounts for the orientational distribution of the resonance field around each knot. For a given orientation and a given resonance field, the additional broadening is proportional to the magnitude of the orientational gradient of the resonance field and to the Voronoi cell area a_{Vor}

$$\tilde{\Gamma} = \sqrt{\Gamma_{\mathrm{tot}}^2 + \alpha a_{\mathrm{Vor}} \left| \frac{\partial B_{\mathrm{res}}}{\partial z_{\mathrm{L}}} \right|^2}. \tag{16}$$

With a suitable choice of the proportionality constant α, simulation noise in the spectrum can be significantly reduced. However, the broadening of the resulting spectrum will be visibly larger than the one specified by the physical broadenings, and spikes might appear at spectral turning points (where the gradient is zero) if the linewidths Γ_{tot} are small. This gradient-smoothing technique is based on a mosaic model for computing broadenings in single crystals [26] and is used in some programs [1,17,22].

The second method, used in EasySpin, is interpolative. Originally, it has been devised for solid-state NMR spectra [34,35], but has only received little attention in EPR [32]. Each Delaunay triangle of the spherical grid on the orientational sphere (see Fig. 2) delimits a set of close orientations with smoothly varying resonance fields, intensities, and widths. Spin systems with orientations within such a triangle give rise to a partial powder spectrum. The sum of these subspectra over all Delaunay triangles gives the total powder spectrum.

The partial powder spectrum due to one Delaunay triangle can be computed analytically [34,35], if it is assumed that, within the triangle, the resonance position varies linearly and that the transition intensity and the linewidth are constant. For sufficiently small triangles, these assumptions hold. In the case of vanishing linewidths, the resulting partial powder spectrum is a sharp triangle (see Fig. 3A), with an area proportional to the average line intensity at the three vertex orientations and to the spherical triangle area a_{Tri}.

This simple geometric projection technique is applicable for isotropic linewidths only. In this case, sharp triangles

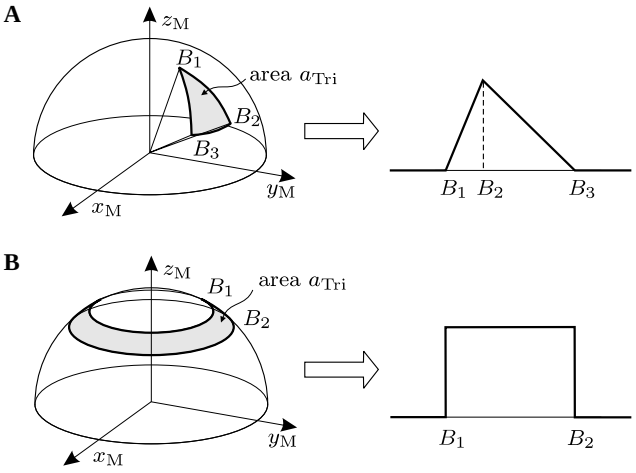

Fig. 3. Interpolative projection method. B_i are resonance fields of a transition. (A) Non-axial symmetry, (B) axial symmetry. All the orientations within the small spherical triangle (zone) on the left give rise to a triangular (rectangular) subspectrum shown on the right.

are summed up, resulting in a stick powder spectrum, which is convoluted with the isotropic line shape. For anisotropic linewidths, each triangle is broadened differently and would have to be convoluted separately with a Gaussian profile. Since these multiple convolutions are impractical, EasySpin implements a fast approximation to perform the combined projection-convolution in a computationally efficient way. Compared to the gradient smoothing scheme, it gives similar results, but does not require the computation of gradients.

In this method, each broadened triangular subspectrum is approximated by a single Gaussian centred at the centre of mass of the triangle $B_{\mathrm{cm}} = (B_1 + B_2 + B_3)/3$ (see Fig. 4). The width $\tilde{\Gamma}$ of the approximating Gaussian is a function of the relative broadening of the subspectrum defined by

$$\lambda_{\mathrm{B}} = \frac{\Gamma_{\mathrm{tot}}}{\Delta B}, \tag{17}$$

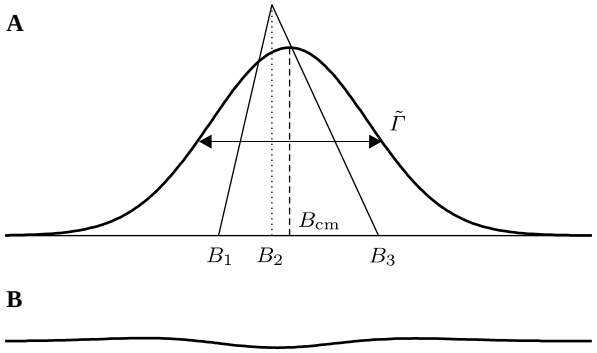

Fig. 4. Approximation of a broadened triangular subspectrum with $\lambda_{\mathrm{B}} = 1$ by a Gaussian line centred at $B_{\mathrm{cm}} = (B_1 + B_2 + B_3)/3$ with least-squares fitted width given by Eq. (18) and $\alpha = 1$: $\Gamma_{\mathrm{approx}}/\Gamma_{\mathrm{tot}} = 1.154$. (A) Triangular spectrum and approximating Gaussian, (B) difference between exact convolution (not shown) and approximating Gaussian, same scale as (A).

where Γ_{tot} is the Gaussian full linewidth at half height from Eq. (13) and $\Delta B = B_3 - B_1$ is the spread of the triangular stick spectrum. We have determined the optimal $\tilde{\Gamma}(\lambda_{\mathrm{B}})$ dependence by least-squares fitting a Gaussian to broadened orthogonal triangles (i.e., $B_1 < B_2 = B_3$). The results follow the simple relationship:

$$\tilde{\Gamma} = \Gamma_{\mathrm{tot}}\left(1 + \alpha\frac{c}{\lambda_{\mathrm{B}}^2}\right) \tag{18}$$

with $c = 0.154$ and $\alpha = 1$. By setting $\alpha = 2$, the smoothing effect can be enhanced without visibly distorting the linewidths in the total powder spectrum, in contrast to the application of Eq. (16).

The relative spectral broadening defined in Eq. (17) is an excellent measure for simulation accuracy and efficiency. $\lambda_{\mathrm{B}} < 0.01$ indicates a stick spectrum with essentially no broadening, whereas $\lambda_{\mathrm{B}} > 1$ means that the spectral anisotropy is invisible. Consequently, in a powder spectrum simulation the smallest broadening encountered in all triangles $\lambda_{\min}$ is a measure of the overall smoothness of the spectrum. If $\lambda_{\min} < 0.5$, significant simulation noise is still visible, $\lambda_{\min} \approx 1$ implies that the spectrum is smooth, and $\lambda_{\min} > 2$ is an indication that the resolution of the orientational grid was higher than necessary.

All methods of spectral construction for anisotropic spin systems require many computationally expensive evaluations of the Gaussian line shape for various widths and positions, which are then added to give the total spectrum. This can be circumvented by using a fast scaled copy procedure [4,36]. In this approach, a single Gaussian is pre-computed to a very high resolution, after which different linewidths are obtained by scaling the abscissa and copying the values from the tabulated line shape to the spectral vector. To further save time, the Gaussian is truncated.

In the case of axial symmetry ($D_{\infty h}$), the projection is simpler than in the general non-axial case discussed above. The orientational sphere is subdivided into spherical zones with $\theta_i \leqslant \theta \leqslant \theta_{i+1}$ (see Fig. 3B), with computed resonance data at $(0, \theta_i)$ and $(0, \theta_{i+1})$. Each spherical zone gives rise to a rectangular stick subspectrum, if the same approximations as in the non-axial case are made. For anisotropic linewidths, each broadened rectangular subspectrum can be approximated by a Gaussian centred at $B_{\mathrm{cm}} = (B_1 + B_2)/2$, where the least-squares fitted width is given by Eq. (18) with $c = 0.231$. Again, $\alpha = 2$ is used for enhanced smoothing.

Fig. 5 illustrates the efficiency of the projection scheme described above compared to a simple summation over the knots of the spherical grid. Relatively few orientations are needed to obtain a smooth powder spectrum: a grid with 136 knots (Fig. 5A) is sufficient to give a spectrum free of artifacts. With 528 knots (Fig. 5B), the spectrum obtained by projection is virtually ripple-free, whereas the sum-over-knots spectrum still features significant simulation noise.

All methods discussed above construct the absorption spectrum. In a cw EPR experiment, first- or second-harmonic spectra are measured. Computationally, they are obtained from the absorption spectrum either by differentiation or by pseudo-modulation (see below).

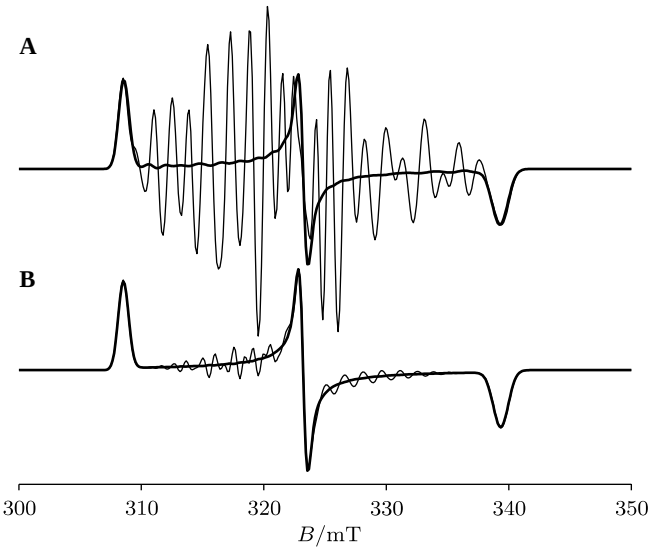

Fig. 5. Simulation of first-harmonic powder spectra using simple summation over knots (thin lines) and the projection technique (thick lines). Parameters: $S = 1/2$, $g = [2.2,2.1,2.0]$, $\nu_{\mathrm{mw}} = 9.5$ GHz, anisotropic frequency-domain linewidths [30,20,40] MHz. (A) $K = 16$, total 136 knots, $\lambda_{\min} = 0.3$, (B) $K = 32$, total 528 knots, $\lambda_{\min} = 0.7$.

2.2. Solution EPR

Although `pepper` supports systems with an arbitrary number of nuclei, the computational effort increases considerably if the state space dimension exceeds about 100. This can happen for organic radicals as well as transition metal complexes. For solid-state spectra, nuclei with small hyperfine couplings can optionally be treated by first-order perturbation theory, as mentioned above.

For liquid-state spectra, EasySpin provides `garlic`, a fast simulation function for isotropic EPR spectra of $S = 1/2$ systems coupled to an arbitrary number of nuclear spins $I \geqslant 1/2$ with hyperfine couplings smaller than the electron Zeeman interaction, governed by the Hamiltonian

$$\mathscr{H}(B) = \frac{\beta_{\mathrm{e}}}{h} g_{\mathrm{iso}} B S_z - \frac{\beta_{\mathrm{n}}}{h} g_{\mathrm{n}} B I_z + a_{\mathrm{iso}} \boldsymbol{S}^{\mathrm{T}} \boldsymbol{I}. \tag{19}$$

Only resonance lines of allowed transitions ($\Delta m_{\mathrm{I}} = 0$) are computed, and all transition intensities are assumed to be equal.

To compute the resonance fields, `garlic` uses the analytical Breit–Rabi expression [37] for the energy levels as a function of the external magnetic field and solves it for B using a fixed-point iteration

$$B_{k+1} = \frac{h a_{\mathrm{iso}}}{\gamma(1 - \xi_k^2)}\left\{-m_{\mathrm{I}} \pm \sqrt{m_{\mathrm{I}}^2 + (1 - \xi_k^2)\left[(2\xi_k)^{-2} - \left(I + \frac{1}{2}\right)^2\right]}\right\} \tag{20}$$

with

$$\xi_k = \frac{a_{\mathrm{iso}}/2}{\nu_{\mathrm{mw}} + \beta_{\mathrm{n}} g_{\mathrm{n}} B_k/h} \quad \gamma = \beta_{\mathrm{e}} g_{\mathrm{iso}} + \beta_{\mathrm{n}} g_{\mathrm{n}}. \tag{21}$$

The sign choice in Eq. (20) depends on the sign of a_{iso}. An excellent starting field value B_0 is obtained directly from Eq. (20) by setting $g_{\mathrm{n}} = 0$. This new method is by far superior to the commonly used evaluation of expressions obtained from perturbation theory, since it quickly converges to the exact resonance field within numerical accuracy, usually after two or three iterations.

To properly simulate spectra with n equivalent nuclei with spin J, they are recoupled to form resultant J spins with $K = nI, nI-1, \ldots,$ which are then treated separately [38]. Sets of equivalent nuclei are treated sequentially, i.e., cross terms are neglected.

If the hyperfine couplings are large ($a_{\mathrm{iso}}(I+1/2) \geqslant 0.2\nu_{\mathrm{mw}}$), cross terms between different nuclei (or groups of equivalent nuclei) will significantly influence the resonance field positions. In addition, the intensities of the allowed transitions are not identical any more, and transitions with $\Delta m_{\mathrm{I}} \neq 0$ can have significant intensity. `garlic` automatically detects this situation, and `pepper` should be used instead, which is accurate for any magnitude of hyperfine couplings, though much slower.

`garlic` can compute spectra in the fast-motion regime using the Kivelson formula for m_{I}-dependent Lorentzian line broadening

$$\Gamma(m_{\mathrm{I}}) = a + b m_{\mathrm{I}} + c m_{\mathrm{I}}^2. \tag{22}$$

The rotational correlation time τ_{rot} can be extracted from the parameters a, b, and c [38].

2.3. Solid-state ENDOR

Solid-state ENDOR spectra are computed by the function `salt`. The structure of the calculation is very similar to that used for solid-state EPR spectra. The powder averaging procedure is identical to the one for EPR spectra with isotropic linewidths.

ENDOR resonance frequencies can be obtained in a much simpler way than EPR resonance fields. Since the external field is constant in an ENDOR experiment, the spin Hamiltonian has to be diagonalized only once for each orientation. The differences of the eigenvalues give the resonance frequencies. Only isotropic ENDOR line broadening is supported. Anisotropic EPR line broadening is taken into account in the ENDOR intensity computation. There, a few peculiarities have to be considered, which are discussed in the following.

The ENDOR line intensity can be written as the product of three factors

$$A_{uv}^{(\mathrm{ENDOR})} = M_{uv}(\boldsymbol{B}_2)\beta_{uv}\alpha_{uv}(\nu_{\mathrm{mw}}). \tag{23}$$

M_{uv} is the ENDOR transition rate between the states u and v, β_{uv} is the polarization factor discussed in Section 2.1.3, and α_{uv} is an additional ENDOR selectivity factor.

The ENDOR transition rate between two nuclear spin states differs from the NMR transitions rate, since the electron magnetic moment almost adiabatically follows the radio frequency (RF) field $\boldsymbol{B}_2$ and thus contributes to the total excitation field at the nucleus, an effect known as hyperfine enhancement [39]. Since this effect is due to the interaction between RF field and electron spin, it is taken into account by including both electron and nuclear Zeeman operators in the expression for the transition rate

$$M_{uv} = B_2^2 |\langle v|G_{x\mathrm{L}}|u\rangle|^2. \tag{24}$$

An ENDOR line between state u and v has non-zero intensity only when the microwave frequency ν_{mw} excites an EPR transition which has a level in common with one of the two states u and v. Hence, the ENDOR intensity is proportional to the sum over all EPR transition moments involving one of the states weighted by the excitation profile of the microwave

$$\alpha_{uv} = \sum_q \sum_{k=u,v} G(\Delta_{qk} - \nu_{\mathrm{mw}}, \Gamma_{\mathrm{mw}}) |\langle q|G_{x\mathrm{L}}|k\rangle|^2. \tag{25}$$

G indicates a Gaussian line, and Γ_{mw} is the bandwidth of the microwave excitation. If the microwave excitation does not hit an EPR transition involving either u or v, this factor vanishes and, as a consequence, the ENDOR transition intensity is zero.

Eq. (25), first used in the program MAGRES [2], describes the fact that ENDOR spectra of anisotropic systems are usually orientation and transition selective, since at a given magnetic field EPR transitions of only a limited subset of orientations can be excited. All other transitions and orientations do not contribute to the ENDOR spectrum.

For simulations of powder spectra, this selectivity of ENDOR is a significant computational burden, since often only a small fraction of computed orientations exhibit an ENDOR response. The majority of orientations are evaluated without giving contributions to the final spectrum. There seems to be no general remedy against this superfluous computations. If the orientation and transition selectivity is determined by the g tensor and by nuclei with large hyperfine couplings, a viable work-around is an orientation pre-selection: α_{uv} is computed for all orientations, but for a reduced spin system containing only spins with anisotropic interactions larger than the excitation bandwidth of the microwave field. In a second step, the ENDOR spectrum of the full system is computed for those orientations only where α_{uv} is above a given threshold. Alternatively, a reduced spin system containing only the nuclei of interest can be used for the ENDOR simulation in this second step [40].

Although the expressions implemented in `salt` are valid for cw ENDOR, the function can be used for the simulation of Davies ENDOR spectra of weakly coupled nuclei without too much error.

3. Other functionality

In this section, additional EasySpin functions are discussed. They represent the building blocks for implementing more complex simulation functions. Many of them are used in the simulation functions `pepper`, `salt`, and `garlic` described above.

Information about a spin system is needed by many functions. Hence, a general specification format for spin systems is provided. A spin system is defined by declaring a Matlab structure with the parameters contained in appropriately named fields. For example

```
CuSystem = struct('S',1/2,'Nucs','63Cu',...
  'g',[2.3 2.3 2],'A',[40 40 470])
```

represents an $S = 1/2$ system coupled to a ^{63}Cu nucleus. 'g' and 'A' define the principal values of the g and A interaction matrices, the latter one in units of MHz. The orientation of the various tensors in the molecular frame can be specified in separate fields in terms of Euler angles. The total spin Hamiltonian from Eq. (1) as well as its individual terms are constructed from this structure by functions like `sham`, `zeeman`, `hfine`, `nquad`, etc. These functions are used by `pepper` as well.

To construct the various spin Hamiltonians necessary for spectral simulations, cartesian spin operators are used. The important function `sop` provides matrix representations of these operators in the standard Zeeman product basis

$$|m_{S1}, m_{S2}, \ldots, m_{I1}, m_{I2}, \ldots\rangle. \tag{26}$$

This is also the basis in which all EasySpin functions operate. `sop` can compute product spin matrices for an arbitrary spin system. For each spin, a cartesian or a shift operator component can be specified. As an example, `sop([1/2 1],'x+')` gives the 6×6 matrix representation of the operator $S_x I_+$ of the two-spin system $S = 1/2$, $I = 1$.

In addition, the function `stev` provides extended Stevens operator matrices O_k^q for arbitrary spins and arbitrary $k \geqslant 0$ and $-k \leqslant q \leqslant k$, using a recently published computation method based on spherical tensor operators and a recursion relation for the normalization factors [7,41].

`levels` and `levelsplot` are functions for computing and plotting energy level diagrams. EPR and ENDOR resonance positions and intensities for a given spin system can be computed using `resfields` and `endorfrq`. Routines for pulse EPR [8] include `evolve` for the evolution of density matrices in time-domain, and `propint`, a function that computes propagators for the evolution under time-independent and time-dependent Hamiltonians [4].

EasySpin functions also cover tasks which are not directly related to spin systems being nevertheless of paramount importance to numerical applications in EPR.

The function `sphgrid` provides spherical grids for a given symmetry as defined by Eq. (15). `sphrand` provides large sets of orientations randomly and uniformly distributed over the entire orientational sphere.

Beyond the common Gaussian and Lorentzian line shape functions (`gaussian` and `lorentzian`), EasySpin provides functions for Voigtian (convolution of Gaussian and Lorentzian; `voigtian`) and pseudo-Voigtian (linear combination of Gaussian and Lorentzian; `lshape`) line shapes [42,43].

EasySpin also features a function that performs pseudo-modulation [44], which consists of a convolution

$$S_{\mathrm{m}}^{(n)}(B) = S(B) * M_n(B, B_{\mathrm{m}}) \tag{27}$$

of the absorption spectrum $S(B)$ with an appropriate kernel function M_n to give the pseudo-modulated spectrum $S_{\mathrm{m}}^{(n)}$, as illustrated in Fig. 6. n is the detection harmonic, and B_{m} is the base-to-peak modulation amplitude. The pseudo-modulation kernel is the inverse Fourier transform of a Bessel function

$$M_n(B, B_{\mathrm{m}}) = \mathrm{i}^n \int_{-\infty}^{\infty} J_n(\beta B_{\mathrm{m}}) \mathrm{e}^{\mathrm{i}\beta B_{\mathrm{m}}}\, \mathrm{d}\beta = (-1)^n \frac{2T_n(B/B_{\mathrm{m}})}{\sqrt{B_{\mathrm{m}}^2 - B^2}}, \tag{28}$$

where T_n is the Chebyshev polynomial of the first kind and of order n [4]. Pseudo-modulation neglects modulation sidebands. By using a more complicated modulation kernel (based on Eq. (64) from [45]), sidebands could be correctly simulated. This, however, is not included in EasySpin, since sidebands are rarely observed and the associated computations are very expensive.

Most common data processing like integration, FFT, etc., can be achieved with built-in Matlab functions. EasySpin extends these capabilities by providing functions for polynomial and exponential fitting used for baseline corrections and relaxation studies (`basecorr`, `exponfit`),

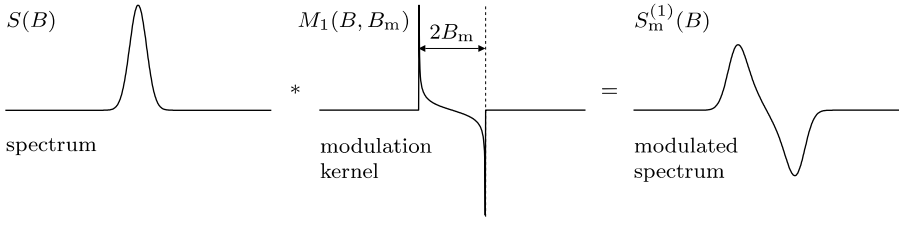

Fig. 6. First-harmonic pseudo-modulation by convolution of the absorption spectrum with a Chebyshev polynomial modulation kernel [4]. $2B_{\mathrm{m}}$ is the peak-to-peak modulation amplitude.

Savitzky–Golay filters [48] for smoothing and differentiation of noisy data (`smooth`), and cross-term averaged FFT (`ctafft`) for removing dead-time artifacts in ESEEM spectra [49]. A digital equivalent to the common RC filter employed in cw EPR spectrometers is also available (`rcfilt`). Experimental spectral data stored in common file formats (Bruker ESP, BES^{3}T) can be imported into Matlab using `eprload`.

A set of functions (`erot`, `eulang`, `vec2ang`, and `ang2vec`) supports inter-conversion between rotation matrices and Euler angles, following the z–y'–z'' convention as defined in [8,38,46]. Angular momentum algebra is supported via functions for recoupling of equivalent spins (`equivsplit`, `equivcouple`) and for the computation of Clebsch-Gordan coefficients, 3-j and 6-j symbols (`clebschgordan`, `wigner3j`, `wigner6j`; [47]).

EasySpin also includes a set of natural constants pertinent to EPR as well as an extensive isotope database containing nuclear spins, g_n values, quadrupole moments and natural abundances for all stable and the most important radioactive nuclides.

4. Examples

In this section, we illustrate how the toolbox can be used to generate EPR data for a variety of complex situations. The results can be visualized with built-in graphical facilities of Matlab. The Matlab/EasySpin code that generates the spectral data for the figures is listed in the Appendix A.

Fig. 7 shows the simulated solution cw EPR spectrum of the bridged biaryl cation radical of 6-hydrodipyrido[1,2-*c*:2′,1′-*e*]-imidazole [50], a typical application of the function `garlic`. The radical contains ten protons and two nitrogens coupled to the unpaired electron, giving a total of 9216 resonance lines in the spectrum. Note that due to the large nitrogen coupling, second-order shifts of approx. 0.01 mT are similar to the linewidth and the smaller hyperfine splittings in the spectrum. Third-order shifts are $\leqslant$0.001 mT. `garlic` computes the spectrum to infinite order using the fixed-point formula Eq. (20). The computation time on a 2 GHz Linux PC was <0.1 s.

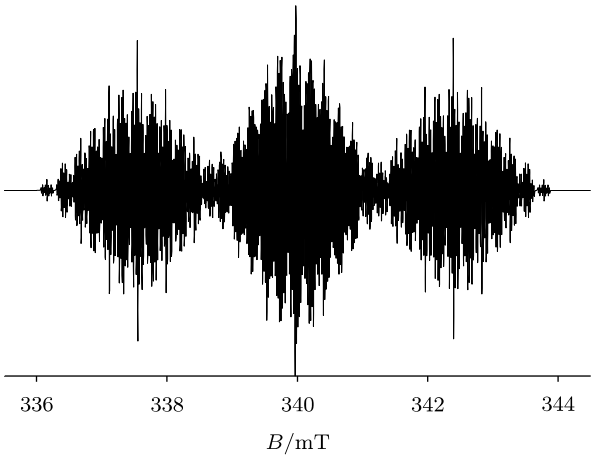

Fig. 7. X-band solution cw EPR spectrum of the cation radical of 6-hydrodipyrido[1,2-*c*:2′,1′-*e*]-imidazole. Parameters: $g_{iso} = 2.00316$, linewidth 0.01 mT, couplings in MHz: N(2) 12.16, H(2) −6.70, H(2) −1.82, H(2) −7.88, H(2) −0.64, H(2) 67.93. $\nu_{mw} = 9.532$ GHz.

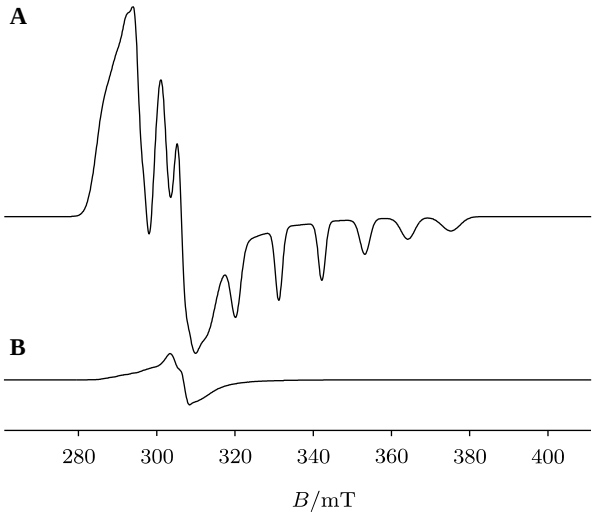

Fig. 8. X-band powder EPR spectrum of a hypothetical Co^{2+} system including A stain broadenings. Parameters: $g = [2.28,2.19,2.01]$, $A = [70,30,309]$ MHz, A strain [45,25,40] MHz, residual broadening 60 MHz. $\nu_{mw} = 9.475$ GHz. (A) Full cw EPR spectrum, (B) contribution from $|\Delta m_I| \neq 1$ transitions.

Some capabilities of the cw EPR simulation function `pepper` are illustrated in Fig. 8. It shows a powder cw EPR spectrum of a typical Co^{2+} complex ($S = 1/2$, $I = 7/2$). The simulation includes frequently observed A strain broadenings, as can be seen from the m_I-dependent linewidths in Fig. 8A. The spectrum contains not only contributions from the eight allowed transitions $|\Delta m_I| = 1$, but from 27 transitions with $|\Delta m_I| \neq 1$ as well. `pepper` can compute separate spectra for each transition, which allows for a separate display of these "forbidden" contributions as shown in Fig. 8B. The simulation took 5 s.

The function `resfields` can be used to generate transition "roadmaps," i.e., plots of the dependence of resonance field positions on the orientation of a paramagnetic centre. Fig. 9 shows the roadmap for an $S = 5/2$ system with axial zero-field splitting in two different representations. The polar (θ, B) representation is the more common one, whereas in the cartesian (B_x, B_z) representation the symmetry of the roadmap is more evident. The high-resolution computation took 25 s.

A series of solid-state ENDOR spectra of a powder sample measured at different values of the static magnetic field is often used to determine hyperfine and quadrupole interactions in disordered systems. As an example, Fig. 10 shows the ENDOR spectra of a proton with an orthorhombic A coupled to an $S = 1/2$ with an orthorhombic g tensor not collinear with the A tensor, simulated with the EasySpin function `salt`. For each magnetic field value, a different set of orientations is selected. `salt` takes

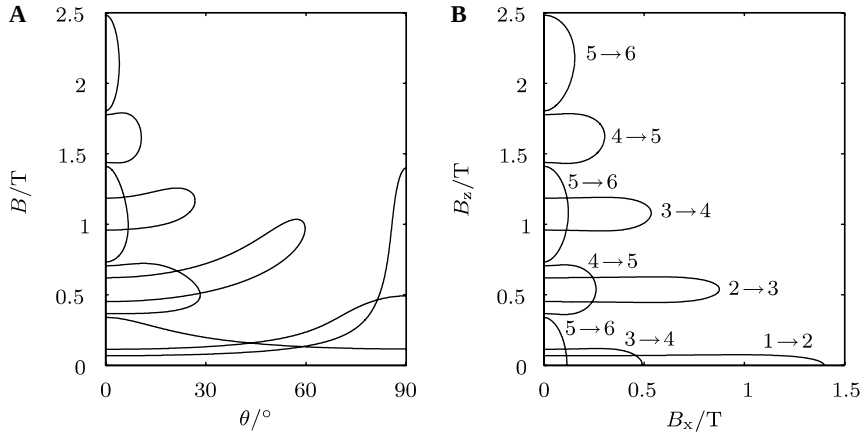

Fig. 9. Transition "roadmap" of an $S = 5/2$ system with $g = 2$ and axial zero-field splitting $D = 5$ GHz for $\phi = 0$ and $0 \leqslant \theta \leqslant \pi/2$, $\nu_{mw} = 9.5$ GHz. (A) Standard polar representation B vs. θ, (B) cartesian representation B_z vs. B_x. The resonance fields are labelled with the associated energy level indices $u \rightarrow v$.

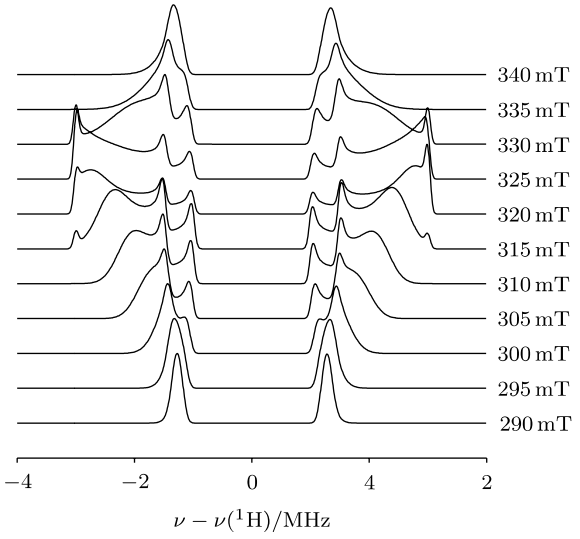

Fig. 10. Powder ENDOR spectra for various field values of an $S = 1/2$ spin with orthorhombic g coupled to a proton with orthorhombic A tensor. Parameters: $g = [2.3,2.1,2]$, $A = [3,6,2]$ MHz, angle between z axes of g and A 45°, $\nu_{mw} = 9.5$ MHz, EPR linewidth 200 MHz, ENDOR linewidth 0.1 MHz, excitation bandwidth 10 MHz.

this into account automatically. Since the tensors in the spin system are not collinear, the field dependence of the ENDOR spectra is quite complex. The total computation time was 5 s.

5. Conclusions

EasySpin combines most of what is known from literature. Its spectral simulation functions `pepper`, `salt`, and `garlic` include a series of improvements and new methods such as automatic determination of spin Hamiltonian symmetry, the adaptive method for resonance field determination, the spectral projection method extended to anisotropic line shapes, and the fixed-point iteration for the Breit–Rabi formula. These methods are designed to increase the robustness and the accuracy of spectral simulations.

A remark is in order about the computational accuracy. Simulations use various natural constants, which have no-zero uncertainty. Of all fundamental constants involved, the Planck constant has the largest relative uncertainty, 10^{-7}. Due to this limiting uncertainty of the Planck constant, spectral line positions cannot be known to more than 7 accurate digits. Most nuclear g values have significantly larger uncertainties than the Planck constant. Thus, to compute resonances and simulate spectra accurately, it is sufficient if all computational algorithms involved have numerical and modelling errors below 10^{-7}.

EasySpin has several advantages over other EPR simulation programs [1,22,17,51]. Since it is based on Matlab, it is interactive, programmable, extensible and features rich support for graphical visualizations. In addition, its functionality is not restricted to a single task like simulating cw EPR spectra. For routine applications, it might be advantageous to use graphical interfaces to EasySpin. These can easily be written in Matlab.

There exist excellent C and C++ libraries for spin physics, the most extensive being Gamma [52] and BlochLib [53], both originally developed for solid-state NMR. They implement most of the basic entities necessary for EPR computations (matrices, tensors, etc.), but lack EPR simulation functionality and visualization capabilities and are not interactive. EasySpin is similar to another program package for solid-state NMR [54].

With all its simulation functionality, EasySpin can be used together with Matlab's optimization functions like `fminsearch` for least-squares fitting of simulated spectra to experimental ones. However, fitting of spectral data, even for cw EPR, is not failsafe and still an active area of research (see, e.g. [55]). The presence of many local minima in the least-squares objective function, the over-parameterization of the model, as well as the diffi-

culty to obtained good starting parameters are currently the main obstacles to routine application of fitting routines.

Currently, EasySpin does not include functions for the simulation of slow-motion spectra [56].

Pulse EPR simulation functionality for one- and two-dimensional experiments is currently under development [4,57]. The main problem of a general pulse EPR simulation function is the high computational cost involved when a brute-force approach is used. Time-saving approximations break down for many systems. E.g., the rotating frame approximation is not generally applicable to high-spin systems, and simulations have to be performed in the laboratory frame. This results in impractically long computation times. A frequency-domain approach along the lines of [58] helps to reduce the computational cost substantially, but significantly increases the complexity of the implementation.

In conclusion, EasySpin represents an extensive and flexible collection of routines for EPR data analysis and spectral simulations. The toolbox should help to transform EPR spectral simulations from a research topic to a easy-to-use research tool. EasySpin can be obtained from http://www.easyspin.ethz.ch, where extensive documentation and a collection of application examples are available, too.

Acknowledgments

This project is supported by the Swiss National Science Foundation. We thank the many EasySpin users worldwide for their valuable feedback.

Appendix A

This Appendix lists the Matlab/EasySpin code for the examples presented in Section 4. Commands for graphical rendering are omitted.

A.1. Example 1

```
A = [12.16 -6.70 -1.82 -7.88 -0.64 67.93]; % MHz
Sys=struct('g',2.00316,'Nucs','14N,1H,1H,1H,1H,1H',...
  'n',[2 2 2 2 2 2],'A',A,'lw',0.01);
Exp = struct('mwFreq',9.532,'nPoints',2^13,...
  'Range',[335.5 344.5]);
[B,spec] = garlic(Sys,Exp);
```

A.2. Example 2

```
g = [2.28 2.19 2.01]; A = [70 30 309];
AStrain = [45 25 40]; residual = [1 1 1]*60;
Sys = struct('S',1/2,'Nucs','59Co','g',g,'A',A,...
  'AStrain',AStrain,'HStrain',residual);
Exp = struct('Range',[261 411],'mwFreq',9.475);
Opt = struct('Output','separate');
[x,y] = pepper(Sys,Exp,Opt);
```

A.3. Example 3

```
Sys = struct('S',5/2,'g',[2 2 2],'D',[1 1 -2]*5e3);
Par = struct('mwFreq',9.5,'Range',[0 5000]);
[phi,theta] = sphgrid('Dinfh',36);
Pos = resfields(Sys,Par,[phi;theta]);
```

A.4. Example 4

```
Sys = struct('S',1/2,'g',[2.3 2.1 2],'Nucs','1H',...
  'A',[3 6 2],'Apa',[0 45 0]*pi/180);
Sys.lwEndor = 0.1; % MHz
Sys.HStrain = [1 1 1]*200; % MHz
Exp = struct('mwFreq',9.5,'ExciteWidth',10);
Opt = struct('nKnots',51);
B = 290:5:340;
nuN = larmorfrq('1H',B);
for k = 1:numel(B)
  Exp.Field = B(k);
  Exp.Range = nuN(k) + [-4 4];
  [x,y{k}] = salt(Sys,Exp,Opt);
end
```

References

[1] M. Griffin, A. Muys, C. Noble, D. Wang, C. Eldershaw, K.E. Gates, K. Burrage, G.R. Hanson, XSophe, a computer simulation software suite for the analysis of electron paramagnetic resonance spectra, Mol. Phys. Rep. 26 (1999) 60–84.

[2] C.P. Keijzers, E.J. Reijerse, P. Stanm, M.F. Dumont, M.C.M. Gribnau, MAGRES: a general program for electron spin resonance, ENDOR and ESEEM, J. Chem. Soc. Faraday Trans. 1 (83) (1987) 3493–3503.

[3] R. Weber, Win-Epr Simfonia Manual, Bruker Instruments Inc., Billerica, MA USA.

[4] St. Stoll, Spectral simulations in solid-state EPR, PhD thesis, ETH Zurich, 2003.

[5] St. Stoll, A. Schweiger, An adaptive method for computing resonance fields for continuous-wave EPR spectra, Chem. Phys. Lett. 380 (2003) 464–470.

[6] J.A. Weil, J.R. Bolton, J.E. Wertz, Electron Paramagnetic Resonance, Wiley, New York, 1994.

[7] C. Rudowicz, C.Y. Chung, The generalization of the extended Stevens operators to higher ranks and spins, and a systematic review of the tables of the tensor operators and their matrix elements, J. Phys. Condens. Matter 16 (2004) 5825–5847.

[8] A. Schweiger, G. Jeschke, Principles of Pulse Electron Paramagnetic Resonance, Oxford University Press, Oxford, 2001.

[9] T. Kato, A Short Introduction to Perturbation Theory of Linear Operators, Springer, Berlin, 1982.

[10] G. Morin, D. Bonnin, Modeling EPR powder spectra using numerical diagonalization of the spin hamiltonian, J. Magn. Reson. 136 (1999) 176–199.

[11] G. van Veen, Simulation and analysis of EPR spectra of paramagnetic ions, J. Magn. Reson. 30 (1978) 91–109.

[12] S.K. Misra, A rigorous evaluation of spin-hamiltonian parameters and linewidths from a polycrystalline EPR spectrum, J. Magn. Reson. 140 (1999) 179–188.

[13] B.J. Gaffney, H.J. Silverstone, Simulation methods for looping transitions, J. Magn. Reson. 134 (1998) 57–66.

[14] G.G. Belford, R.L. Belford, J.F. Burkhalter, Eigenfields: a practical direct calculation of resonance fields and intensities for field-swept fixed-frequency spectrometers, J. Magn. Reson. 11 (1973) 251–265.

[15] S.K. Misra, Evaluation of spin-hamiltonian parameters from EPR data by the method of least-squares fitting, J. Magn. Reson. 23 (1976) 403–410.
[16] K.E. Gates, M. Griffin, G.R. Hanson, K. Burrage, Computer simulation of magnetic resonance spectra employing homotopy, J. Magn. Reson. 135 (1998) 103–112.
[17] J. Glerup, H. Weihe, Magnetic susceptibility and EPR spectra of μ-Cyano-bis[pentaaminechromium(II)] perchlorate, Acta Chem. Scand. 45 (1991) 444–448.
[18] F.E. Mabbs, D. Collison, Electron Paramagnetic Resonance of d Transition Metal Compounds, Studies in Inorganic Chemistry, vol. 16, Elsevier, Amsterdam, 1992.
[19] J.M. Baker, J.R. Chadwick, G. Garton, J.P. Hurrell, E.p.r. and Endor of Tb^{4+} in Thoria, Proc. Roy. Soc. London A 286 (1965) 352–365.
[20] E. Wasserman, L.C. Snyder, W.A. Yager, ESR of the triplet states of randomly oriented molecules, J. Chem. Phys. 41 (1964) 1763–1772.
[21] C.C. Felix, S.I. Weissman, Absence of interference in photoexcitation of triplets, Proc. Natl. Acad. Sci. USA 72 (1975) 4203–4204.
[22] M. Shiotani, in: A. Lund (Ed.), EPR of Free Radicals in Solids, Kluwer Press, 2003.
[23] W. Froncisz, J.S. Hyde, Broadening by strains of lines in the *g*-parallel region of Cu^{2+} EPR spectra, J. Chem. Phys. 73 (1980) 3123–3131.
[24] W.R. Hagen, D.O. Hearshen, R.H. Sands, W.R. Dunham, A statistical theory of powder EPR in distributed systems, J. Magn. Reson. 61 (1985) 220–232.
[25] A. Aqualino, A.S. Brill, G.F. Bryce, B.S. Gerstman, Correlated distributions in *g* and *A* tensors at a biologically active low-symmetry cupric site, Phys. Rev. A 44 (1991) 5257–5271.
[26] R.F. Wenzel, Y.W. Kim, Linewidth of the electron paramagnetic resonance of $(Al_2O_3)_{1-x\,(Cr_2O_3)x}$, Phys. Rev. 140 (1965) A1592–A1598.
[27] E.R. Feher, Sensitivity consideration in microwave paramagnetic resonance absorption techniques, Phys. Rev. A 1A (1964) A145–A157.
[28] J.R. Pilbrow, Lineshapes in frequency-swept and field-swept EPR of spin 1/2, J. Magn. Reson. 58 (1984) 186–203.
[29] R. Aasa, T. Vänngård, EPR signal intensity and powder shapes: a reexamination, J. Magn. Reson. 19 (1975) 308–315.
[30] J.R. Pilbrow, G.R. Sinclair, D.R. Hutton, G.J. Troup, Asymmetric lines in field-swept EPR: Cr^{3+} looping transitions in Ruby, J. Magn. Reson. 52 (1983) 386–399.
[31] M. Bak, N.C. Nielsen, REPULSION, a novel approach to efficient powder averaging in solid-state NMR, J. Magn. Reson. 125 (1997) 181–190.
[32] A. Ponti, Simulation of magnetic resonance static powder lineshapes: a quantitative assessment of spherical codes, J. Magn. Reson. 138 (1999) 288–297.
[33] U. Segre, L. Pasimeni, M. Ruzzi, Simulation of EPR and time resolved EPR lineshapes in partially ordered glasses, Spectrochim. Acta A 56 (2000) 265–271.
[34] H. Ebert, J. Abart, J. Voitländer, Simulation of quarupole disturbed NMR field spectra by using perturbation theory and the triangle integration method, J. Chem. Phys. 79 (1983) 4719–4723.
[35] D.W. Alderman, M.S. Solum, D.M. Grant, Methods for analyzing spectroscopic line shapes. NMR solid powder patterns, J. Chem. Phys. 84 (1986) 3717–3725.
[36] W.R. Hagen, D.O. Hearshen, L.J. Harding, W.R. Dunham, Quantitative numerical analysis of *g* strain in the EPR of distributed systems and its importance for multicenter metalloproteins, J. Magn. Reson. 61 (1985) 233–244.
[37] J.A. Weil, The analysis of large hyperfine splittings in paramagnetic resonance spectroscopy, J. Magn. Reson. 4 (1971) 393–399.
[38] N.M. Atherton, Principles of Electron Spin Resonance, Prentice Hall, 1993.
[39] A. Schweiger, Electron nuclear double resonance of transition metal complexes with organic ligands, Struct. Bonding 51 (1982) 1.
[40] Z. Mádi, S. Van Doorslaer, A. Schweiger, Numerical simulation of one- and two-dimensional ESEEM experiments, J. Magn. Reson. 154 (2002) 181–191.
[41] I.D. Ryabov, On the generation of operator equivalents and the calculation of their matrix elements, J. Magn. Reson. 140 (1999) 141–145.
[42] J.-P. Grivet, Accurate numerical approximation to the Gauss–Lorentz lineshape, J. Magn. Reson. 125 (1997) 102–106.
[43] S.D. Bruce, J. Higinbotham, I. Marshall, P.H. Beswick, An analytical derivation of a popular approximation of the Voigt function for quantification of NMR spectra, J. Magn. Reson. 142 (2000) 57–63.
[44] J.S. Hyde, M. Pasenkiewicz-Gierula, A. Jesmanowicz, W.E. Antholine, Pseudo field modulation in EPR spectroscopy, Appl. Magn. Reson. 1 (1990) 483–496.
[45] M. Kälin, I. Gromov, A. Schweiger, The continuous wave electron paramagnetic resonance experiment revisited, J. Magn. Reson. 160 (2003) 166–182.
[46] J.J. Sakurai, Modern Quantum Mechanics, Addison-Wesley, Reading, MA, 1985.
[47] L.C. Biedenharn, J.D. Louck, Angular Momentum in Quantum Physics, Addison-Wesley, Reading, MA, 1981.
[48] W.H. Press, S.A. Teukolsky, W.T. Vetterling, B.P. Flannery, Numerical Recipes in C++, second ed., Cambridge University Press, Cambridge, 2002.
[49] S. Van Doorslaer, G. Sierra, A. Schweiger, Dead time-dependent line distortions in absolute-value electron spin echo envelope modulation spectra, J. Magn. Reson. 136 (1999) 152–158.
[50] P.D. Sullivan, J.Y. Fong, M.L. Williams, Electron paramagnetic resonance studies of bridged biaryl cation radicals, J. Phys. Chem. 82 (1978) 1181–1185.
[51] M.J. Mombourqette, J.A. Weil, Simulation of magnetic resonance powder spectra, J. Magn. Reson. 99 (1992) 37–44.
[52] S.A. Smith, T.O. Levante, B.H. Meier, R.R. Ernst, Computer simulations in magnetic resonance—an object-oriented programming approach, J. Magn. Reson. A 106 (1994) 75–105.
[53] W.B. Blanton, BlochLib: a fast NMR C++ tool kit, J. Magn. Reson. 162 (2003) 269–283.
[54] M. Bak, J.T. Rasmussen, N.C. Nielsen, SIMPSON: a general simulation program for solid-state NMR spectroscopy, J. Magn. Reson. 147 (2000) 296–330.
[55] T. Spałek, P. Pietrzyk, Z. Sojka, Application of the genetic algorithm joint with the Powell method to nonlinear least-squares fitting of powder EPR spectra, J. Chem. Inf. Model. 45 (2005) 18–29.
[56] D.J. Schneider, J.H. Freed, Calculating slow motional magnetic resonance spectra: a user's guide, Biol. Magn. Reson. 8 (1989) 1–76.
[57] St. Stoll, A. Schweiger, Rapid construction of solid-state magnetic resonance powder spectra from frequencies and amplitudes as applied to ESEEM, J. Magn. Reson. 163 (2003) 248–256.
[58] T. Charpentier, C. Fermon, J. Virlet, Efficient time propagation technique for MAS NMR simulation: application to quadrupolar nuclei, J. Magn. Reson. 132 (1998) 181–190.